ACS Catalysis

Research Article

Cite This: ACS Catal. 2019, 9, 9350−9358

pubs.acs.org/acscatalysis

Pt/Pd Single-Atom Alloys as Highly Active Electrochemical Catalysts and the Origin of Enhanced Activity

Lei Zhang,[†,⊥] Hanshuo Liu,[‡,⊥] Sihang Liu,[§,⊥] Mohammad Norouzi Banis,[†] Zhongxin Song,[†] Junjie Li,[†] Lijun Yang,[∥] Matthew Markiewicz,[∥] Yang Zhao,[†] Ruying Li,[†] Matthew Zheng,[†] Siyu Ye,[∥] Zhi-Jian Zhao,*[,§] Gianluigi A. Botton,*[,‡] and Xueliang Sun*[,†]

[†]Department of Mechanical and Materials Engineering, The University of Western Ontario, London, ON N6A 5B9, Canada

[‡]Department of Materials Science and Engineering, McMaster University, Hamilton, ON L8S 4L8, Canada

[§]Key Laboratory for Green Chemical Technology of Ministry of Education, School of Chemical Engineering and Technology, Collaborative Innovation Center of Chemical Science and Engineering (Tianjin), Tianjin University, Tianjin 300072, P. R. China

[∥]Ballard Power Systems Inc., 9000 Glenlyon Parkway, Burnaby, BC V5J 5J8, Canada

Supporting Information

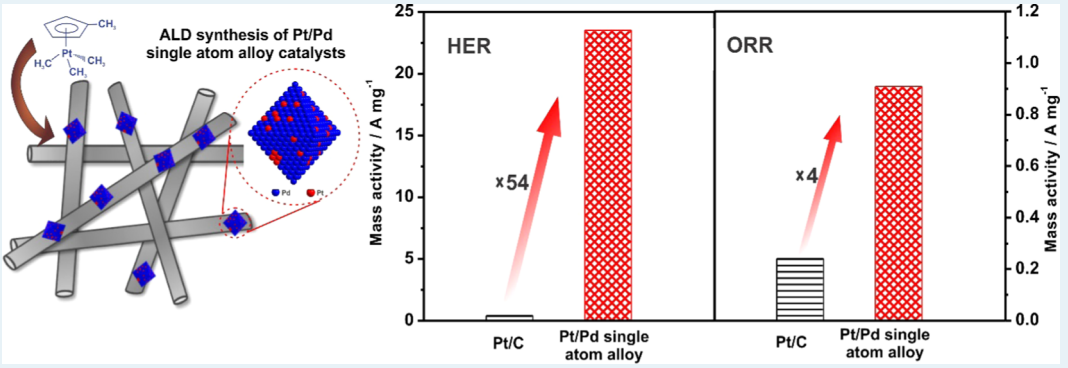

ABSTRACT: Pt single-atom catalysts are receiving more and more attention due to their different properties compared with nanostructures. As one typical kind of single-atom catalysts, Pt-based single-atom alloys (SAAs) have generated significant interest due to their application in several heterogeneous catalytic reactions. However, almost all of the reported Pt-based SAAs are on Cu surface. In addition, it is still great challenge to apply Pt single-atom alloys in electrocatalytic reactions. Herein, we demonstrated a fabrication of Pt/Pd SAA catalysts on nitrogen-doped carbon nanotubes by atomic layer deposition. The as-prepared octahedral Pt/Pd SAA catalysts exhibited greatly improved activity compared to commercial Pt/C catalysts for electrochemical catalytic reactions. According to the X-ray adsorption spectrum, the Pt atoms in Pt/Pd SAA catalysts exhibited higher unoccupied 5d character density of states and a lower Pt−Pt coordination number, compared to those in core−shell structures. In addition, we used density functional theory calculation results to explain the enhanced mechanism of Pt/Pd SAA catalysts for electrochemical reactions. This study opens up an avenue of developing different types of Pt-based catalysts for electrocatalytic reactions and brings insight understanding about catalytic performances of SAA catalysts.

KEYWORDS: *platinum, single-atom alloys, atomic layer deposition, X-ray adsorption spectrum analysis, hydrogen evolution reaction, oxygen reduction reaction*

1. INTRODUCTION

Pt-based catalysts exhibited great electrochemical performance in both anode and cathode of proton exchange membrane fuel cells.[1−5] However, the high cost of Pt-based catalysts has inspired researchers to look for more effective routes to further enhance its activity. Among various methods for reducing the Pt loading, one of the most direct routes is to increase their atom utilization efficiency (AUE) by preparing nanosized particles and clusters or even single-atom catalysts.[6,7] Up to date, several types of Pt single-atom catalysts have been synthesized via a wetness impregnation method,[8−10] coprecipitation method,[11] atomic layer deposition method (ALD),[12−14] and other methods.[15−17]

For electrochemical applications, many studies deposited isolated Pt atoms on carbon-based support, such as graphene, metal−organic framework-derived porous carbon, etc. In addition to carbon support, the Pt single atoms can also be located on the surface of a different metal, which is named as single-atom alloy (SAA). As one typical kind of single-atom

Received: April 24, 2019
Revised: September 4, 2019
Published: September 5, 2019

DOI: 10.1021/acscatal.9b01677
ACS Catal. 2019, 9, 9350−9358

catalysts, Pt-based SAAs have generated significant interest due to their application in several selective hydrogenation/dehydrogenation reactions.[18−22] The Pt single-atom alloys were created by depositing isolated Pt atoms on another metal surface. For example, Gong and co-workers atomically diluted Pt atoms on Cu surfaces. The as-prepared Pt/Cu SAA catalyst exhibited a propylene selectivity of ∼90% in the catalytic dehydrogenation of propane.[22] However, almost all of the reported Pt-based single-atom alloys are on Cu surface. In addition, it is still a great challenge to apply Pt single-atom alloys in electrocatalytic reactions. Pd is an ideal substrate to deposit isolated Pt atoms, as they have similar lattice constants.[23−26] Furthermore, the coordination environment and catalytic activity of Pt atoms can be tuned by deposition on Pd particles with different exposed surfaces.[27−29] Hence, with the formation of Pt/Pd SAA structure, the electrocatalytic activities of Pt atoms can be improved due to the synergistic effect of Pt and Pd.

Herein, we demonstrated the fabrication of Pt/Pd SAA catalysts through an ALD method. The Pt atoms were successfully deposited on Pd nanoparticles with (100) and (111) surfaces, respectively. Interestingly, Pt/Pd SAA catalysts formed on octahedral Pd surfaces. The as-prepared Pt/Pd SAA catalysts exhibited much higher hydrogen evolution reaction (HER) and oxygen reduction reaction (ORR) activities than other types of ALD-prepared Pd−Pt catalysts and commercial Pt/C catalysts. Furthermore, the enhanced mechanism of SAA catalysts was investigated by X-ray absorption spectrum and density functional theory (DFT) calculations.

2. EXPERIMENTAL SECTION

2.1. Preparation of Pd Nanocubes and Octahedrons on Nitrogen-Doped Carbon Nanotube (NCNT). First, we mixed poly(vinylpyrrolidone) (PVP) (105 mg, M_w = 10 000), ascorbic acid (AA, 60 mg), KBr (600 mg), and deionized water (8 mL) in a 20 mL capped vial. The mixture was kept at 80 °C for 10 min, and then 19 mg mL^{-1} Na_2PdCl_4 (3 mL) was injected into the solution. After 3 h, the samples were washed three times with water. For the preparation of Pd octahedrons, we mixed 105 mg PVP, 100 μL HCHO, 0.3 mL Pd cubic seeds, and 8 mL deionized water in a 20 mL capped vial. Then, a 3 mL solution containing 29.0 mg Na_2PdCl_4 was introduced into the solution and kept at 60 °C for 3 h.[30] The samples were washed three times with water to remove PVP. We prepared NCNTs by ultrasonic spray pyrolysis according to a previous paper.[31] The Pd particles were loaded onto NCNTs by ultrasonic method, and the Pd loading amount is 20%.

2.2. Synthesis of Pt SAA Catalysts and Core−Shell Structures on Pd/NCNTs by ALD. Pt was deposited on the Pd nanocubes and octahedrons/NCNTs by ALD (Savannah 100, Cambridge Nanotechnology Inc.). The trimethyl-(methylcyclopentadienyl)-platinum(IV) ($MeCpPtMe_3$) was used as the precursor. We used high-purity N_2 (99.9995%) as the purging gas and carrier gas. The container for $MeCpPtMe_3$ was kept at 65 °C. The chamber temperature was 230 °C. Since ALD valves can only be opened for 30 s at a time, a 2 min exposure of Pt precursor consisted of four 30 s pulses separated by a 10 s purge. To quantitatively analyze the loading amount of Pd and Pt, we dissolved the samples in hot fresh aqua regia overnight and filtered. Then, we used an inductively coupled plasma optical emission spectrometer (ICP-OES) to determine the concentration of Pd and Pt.

2.3. Electrochemical Measurements. The electrochemical measurements were performed in a three-electrode system. We used a glassy carbon rotating-disk electrode (Pine Instruments), a graphite electrode, and a reversible hydrogen electrode (RHE) as the working, counter, and reference electrodes, respectively. We added 3 mg of the as-prepared Pd−Pt/NCNTs into a mixture of deionized water (1.6 mL), isopropanol (0.4 mL, Sigma-Aldrich), and Nafion (5% solution, Sigma-Aldrich, 40 μL) to obtain the ink. Then, the ink was treated by sonication for 10 min before the electrochemical measurement. Ink (20 μL) was loaded onto the glassy carbon electrode for every test. The cyclic voltammograms (CVs) were recorded by cycling between 0.05 and 1.1 V_{RHE} at a scan rate of 0.05 V s^{-1}. The HER test was carried out with a scan rate of 2 mV s^{-1} at a rotation speed of 1600 rpm. The ORR polarization curves with *iR* compensation were carried out in an O_2-saturated electrolyte with a scan rate of 10 mV s^{-1} and a rotation speed of 1600 rpm. The commercial Pt/C (Johnson Matthey Corp., 10 wt %) was tested as the contrast catalyst under the same condition.

2.4. Instrumentation. The characterization of the products was carried out by scanning electron microscopy (SEM, S-4800) and transmission electron microscopy (an FEI Titan Cubed 80−300 kV microscope equipped with spherical aberration correctors at 200 kV). The scanning transmission electron microscopy (STEM) images were collected by a high-angle annular dark-field detector (HAADF). The electron energy loss spectroscopy (EELS) data were acquired by a K2 summit direct detection camera at a 0.5 eV/channel dispersion.

2.5. X-ray Absorption Spectroscopy. We conducted the X-ray absorption near-edge structure (XANES) measurements of the Pt L3- and L2-edges at the hard X-ray microanalysis (HXMA) beamline at the Canadian Light Source (CLS) 06ID-01. The fluorescence yield mode with a solid-state detector was used for obtaining the spectra of each sample. High-purity Pt metal foil was collected in transmission mode for comparison and monochromatic energy calibration. Athena software was used to analyze the obtained X-ray adsorption spectrum (XAS) data. The extracted extended X-ray absorption fine structure (EXAFS) data was weighted by k^3 to obtain the magnitude plots of the EXAFS spectra in radial space. The data was fitted using Artemis software.

2.6. DFT Calculations. We used the plane wave-based Vienna ab initio simulation package to perform the density functional theory (DFT) calculations.[32] To describe the adsorbate adsorption on Pt or Pd atoms, the BEEF−vdW functional was used in the combination with the generalized gradient approximation.[33] Due to the small mismatch of lattice constants of Pt and Pd, the Pt deposition process was simulated by the replacement of the surface Pd atoms directly.[34] A 400 eV energy cutoff and a force convergence standard of 0.02 eV $Å^{-1}$ were qualified to calculate the system. The calculations for OH and H binding energies were performed using a 2 × 2 surface unit cell. The *k*-point mesh was carefully tested, and finally, 3 × 3 × 1 was chosen to sample the Brillouin zone for all calculations. The nanoscale Pt−SAA loaded at Pd octahedra was modeled with five layer slabs of Pd(111), with a surface Pd atom replaced by a Pt atom; the bottom two layers were fixed at the optimized bulk lattice constant of Pd and the top three layers were allowed to relax. The Pt overlayer loaded on Pd cubes was modeled with five layer slabs of Pd(100), with the top layer replaced by a Pt overlayer; the bottom two layers were fixed at the optimized

DOI: 10.1021/acscatal.9b01677
ACS Catal. 2019, 9, 9350−9358

bulk structure. To prevent periodic interaction, a 15 Å spacing was used in the Z direction. The entropies and zero-point energies of surface species were calculated from the vibrational frequencies obtained by DFT using the harmonic oscillator approximation.

The binding energy of OH (BE_{OH}) was calculated as the difference in energy between the total energy of the slab with OH (E_{total}) and the clean slab energy (E_{slab}) and gas-phase OH (E_{OH}): $BE_{OH} = E_{total} - E_{slab} - E_{OH}$. The average adsorption energy of H ($E_{avg\ H}$) is calculated as $E_{avg\ H} = (E_{total} - E_{slab} - nE_H)/n$; E_{total} here is the total energy of the slab with n H*. The differential adsorption energy of H ($E_{diff\ H}$) is calculated as $E_{diff\ H} = E_{total\_n} - E_{total\_n-1} - E_H$; E_{total_n} here is the total energy of the slab with n H* and E_{total_n-1} here is the total energy of the slab with $n - 1$ H*.

Previous studies have shown that the improved specific activity can be attributed to weaken the binding energy of adsorbed OH relative to that on Pt through introducing lattice strain effects and/or ligand effects.[35−37] Therefore, the rate constant k_i for OH hydrogenation on surface i relative to the core−shell models was calculated as $k_i = \exp(-(BE_{OH1} - BE_{OH2})/k_BT)$, where BE_{OH1} is the binding energy of OH on Pt−SAA/Pd(111), BE_{OH2} is the binding energy of OH on Pt−OL/Pd(100), and k_B is the Boltzmann constant; T is 298 K here.

3. RESULTS AND DISCUSSION

3.1. Preparation of Pt/Pd SAA Catalysts by ALD. Pd nanocubes and octahedrons were prepared according to a past reported method (Figure S1).[30] To investigate the Pt deposition on shape-controlled Pd particles, we initially dispersed the Pd particles on silicon wafer substrates and carried out the traditional Pt ALD process by introducing trimethyl(methylcyclopentadienyl)-platinum(IV) ($MeCpPtMe_3$) and O_2 alternately. As shown in Figures S2 and S3, the Pt atoms were successfully deposited on the Pd surfaces after several Pt ALD cycling numbers. To avoid the aggregation of Pd particles during the ALD process, NCNTs with a diameter ranging from 50 to 150 nm were employed as the substrate.[31] The shape-controlled Pd particles were loaded onto NCNT surface by a 30 min ultrasonic to achieve the Pd/NCNT support for Pt deposition.

ALD synthesis of Pt atoms on shape-controlled Pd/NCNT support was obtained using $MeCpPtMe_3$ as the precursor for a 2 min dosing time. As shown in Figure S4, after pulsing $MeCpPtMe_3$ for 2 min at 250 °C, no obvious Pt clusters can be observed on either cubic or octahedral Pd particles from the SEM images. Figure 1a,b displays high-angle annular dark-field scanning transmission electron microscopy (HAADF-STEM) images of Pt/Pd SAA catalysts, which was obtained by treating octahedral Pd/NCNTs with a 2 min Pt dosing time. Note that the contrast of the HAADF-STEM image is highly related to the atomic number of the elements. In this case, the Pt atoms show a brighter contrast compared to the Pd atoms. As seen from Figure 1a, the Pd octahedra were well deposited on the NCNTs. The morphology of the Pd particles was not changed after the ALD of Pt. The atomic-resolution STEM image (Figure 1b) clearly illustrates the presence of a few brighter atoms at the surface of the octahedral Pd particle, suggesting the presence of Pt clusters on the Pd octahedral particle seed. In addition, we also observed some individual bright spots on the surface of octahedral Pd particles, indicating the formation of Pt isolated atoms on Pd surfaces (Figure 1c). The extended

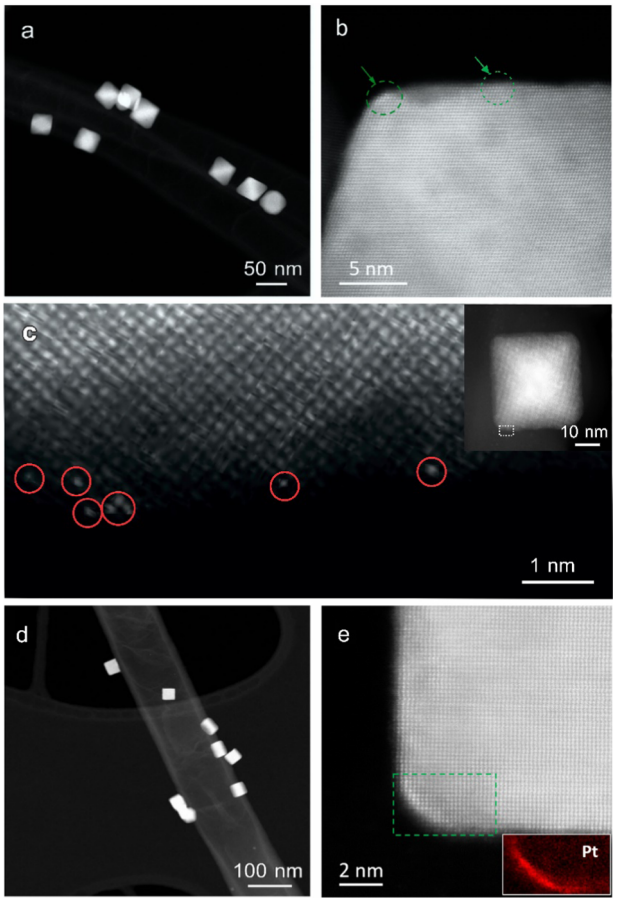

Figure 1. (a) Low-magnification STEM image of the octahedral Pt/Pd SAA catalysts on NCNTs. (b) Atomic-resolution STEM image of an individual octahedral Pt/Pd SAA particle. (c) High-resolution STEM image showing the surface of one individual octahedral Pt/Pd SAA (inset), indicating the formation of Pt isolated atoms on Pd particles. (d) Low-magnification STEM image of the cubic Pd@Pt particles on NCNTs. (e) Atomic-resolution STEM image of cubic cubic Pd@Pt particles. The inset of (e) shows the Pt EELS map.

X-ray absorption fine structure (EXAFS) results further indicate the presence of Pt isolated atoms and clusters on the octahedral Pd−2 min Pt sample, which will be discussed below. The cubic Pd particles also maintained their shape after a 2 min Pt pulse time (Figure 1d,e). As shown in Figure 1d, the edge and the corner of the cubic Pd particle are brighter than those of the bulk, suggesting that a thin layer of Pt with a thickness of about 2−3 atomic layers has been formed on the cubic Pd surface and has a higher concentration at the corner (denoted hereafter as cubic Pd@Pt catalysts). The inset Pt map in Figure 1d further confirms the presence of Pt on the Pd particle. The different deposition phenomenon of Pt on octahedral and cubic Pd nanoparticles was due to the different surface energy of {111} and {100}. As we know, the surface energy of {100} is higher than that of {111}. The higher surface energy might adsorb more Pt precursors on their surface and thus forming a uniform shell. While {111} surface tends to adsorb less amount of precursors, resulting in the isolated Pt atoms. The ICP-OES results showed that the mass ratios between Pt and Pd are 5.6 and 11.1% for the octahedral Pt/Pd SAA catalysts and cubic Pd@Pt catalysts, respectively. The total Pt loading amounts are 1.1 and 2.2 wt %, as shown in Table S1.

DOI: 10.1021/acscatal.9b01677
ACS Catal. 2019, 9, 9350−9358

Table 1. Comparison of the Metal Loading Amount, Electrochemical Surface Area (ECSA), Specific Activity (SA), and Pt Mass Activity (MA_{Pt}) for the As-Prepared Catalysts and Pt/C

	weight percent					
sample	Pd	Pt	Pd + Pt	ECSA ($m^2\ g_{Pt}^{-1}$)	SA at 0.9 V_{RHE} ($mA\ cm_{Pt}^{-2}$)	MA_{Pt} at 0.9 V_{RHE} ($A\ mg_{Pt}^{-1}$)
octahedral Pt/Pd SAA	19.6	2.2	21.8	32.4	0.12	0.91
cubic Pd@Pt catalysts	19.6	1.1	21.8	26.1	0.02	0.04
octahedral Pd−30 min Pt	16.6	16.7	33.3	27.2	0.67	0.36
cubic Pd−30 min Pt	16.4	17.8	34.2	22	0.25	0.14
Pt/C		10%	10%	63.4	0.40	0.24

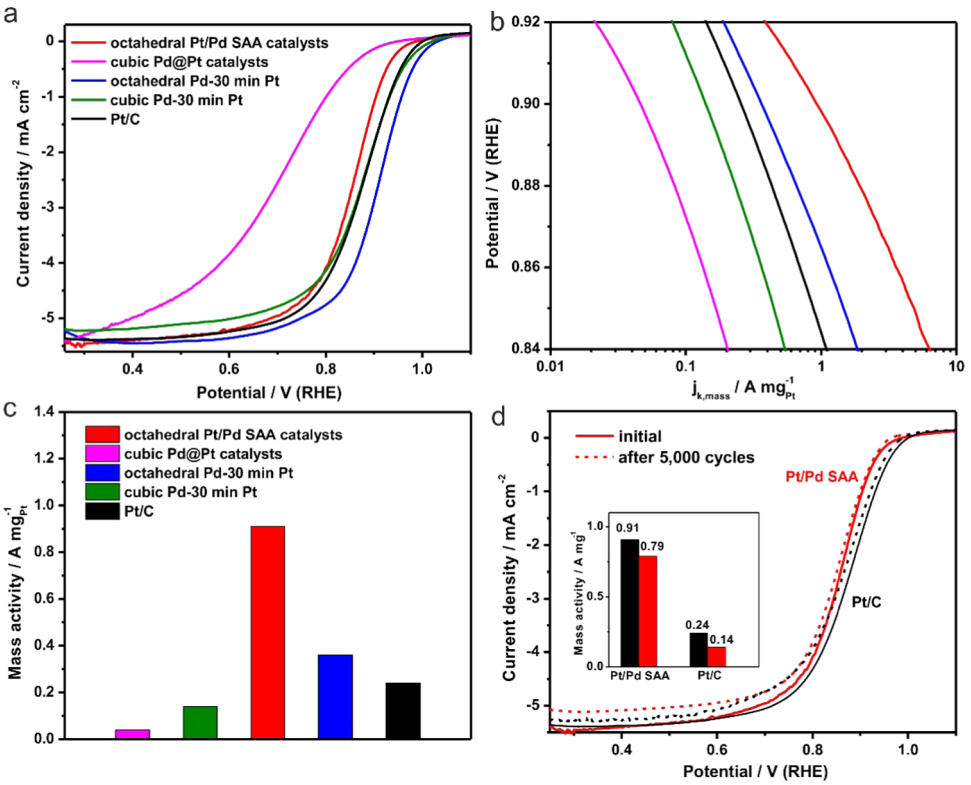

Figure 2. (a) ORR polarization curves of the octahedral Pt/Pd SAA catalysts (octahedral Pd−2 min Pt), cubic Pd@Pt catalysts (cubic Pd−2 min Pt), octahedral Pd−30 min Pt, and cubic Pd−30 min Pt in comparison with a commercial Pt/C catalyst. Catalysts of 6 μg were loaded on rotating disk electrode (RDE), and the current densities were normalized to the geometric area of the RDE (0.196 cm^2). The color scheme applies to (b). (b) Mass activities given as kinetic current densities (j_k) normalized by the mass of Pt. (c) Mass activities of the catalysts at 0.9 V_{RHE}. (d) ORR polarization curves of the octahedral Pt/Pd SAA catalysts and commercial Pt/C before and after accelerated durability test. The inset in d shows the mass activities of the octahedral Pt/Pd SAA catalysts and Pt/C catalysts at 0.9 V_{RHE}.

When the ALD dosing Pt time was increased to 30 min, Pt small clusters with a size of a few nanometers were observed on the surface of both the octahedral Pd and NCNTs (denoted hereafter as octahedral Pd−30 min Pt) (Figure S5a,b). While for the cubic Pd substrates, both thin shell of Pt and individual Pt clusters were observed on the surface of cubic Pd (denoted hereafter as cubic Pd−30 min Pt), as shown in Figure S5c,d. It was observed that the size of Pt particles/atom clusters of the 30 min samples increased, compared to that of shorter pulse time (2 min) samples discussed above. Based on the previous literature, it has been suggested that Pt atom growth during the ALD occurs via combustion of organic ligands during exposure to an oxidant. The result indicated that once a Pt atom/small cluster is formed on the surface, further decomposition of supplied $MeCpPtMe_3$ precursor may occur readily, resulting in the formation of larger Pt clusters.

3.2. Electrochemical Performance of the Pt/Pd SAA Catalysts. We first evaluated the ORR performance of the as-prepared catalysts. Cyclic voltammograms (CVs) for the octahedral Pt/Pd SAA catalysts, cubic Pd@Pt catalysts, octahedral Pd−30 min Pt, cubic Pd−30 min Pt catalysts, and commercial Pt/C were measured in 0.10 M aqueous $HClO_4$. The hydrogen desorption peak is constituted of both exposed Pt and Pd (Figure S6). Therefore, we calculated the electrochemical active surface area (ECSA) of platinum group metal content (Pt + Pd) through hydrogen desorption peak (Table 1). First, we compared the performance of octahedral Pt/Pd SAA catalysts with pure octahedral Pd on NCNTs (Figure S7a). The polarization curve showed that the octahedral Pd exhibited much worse ORR activity than that of the octahedral Pt/Pd SAA catalysts. In addition, the electrochemical impedance spectroscopy (Figure S8) shows that the Pd/NCNT exhibited higher resistance, which resulted in the mass transport limited region. At 0.9 V vs RHE, the current density for the octahedral Pd was almost 0, indicating that the activity of octahedral Pt/Pd SAA catalysts was mostly due to Pt

DOI: 10.1021/acscatal.9b01677
ACS Catal. 2019, 9, 9350−9358

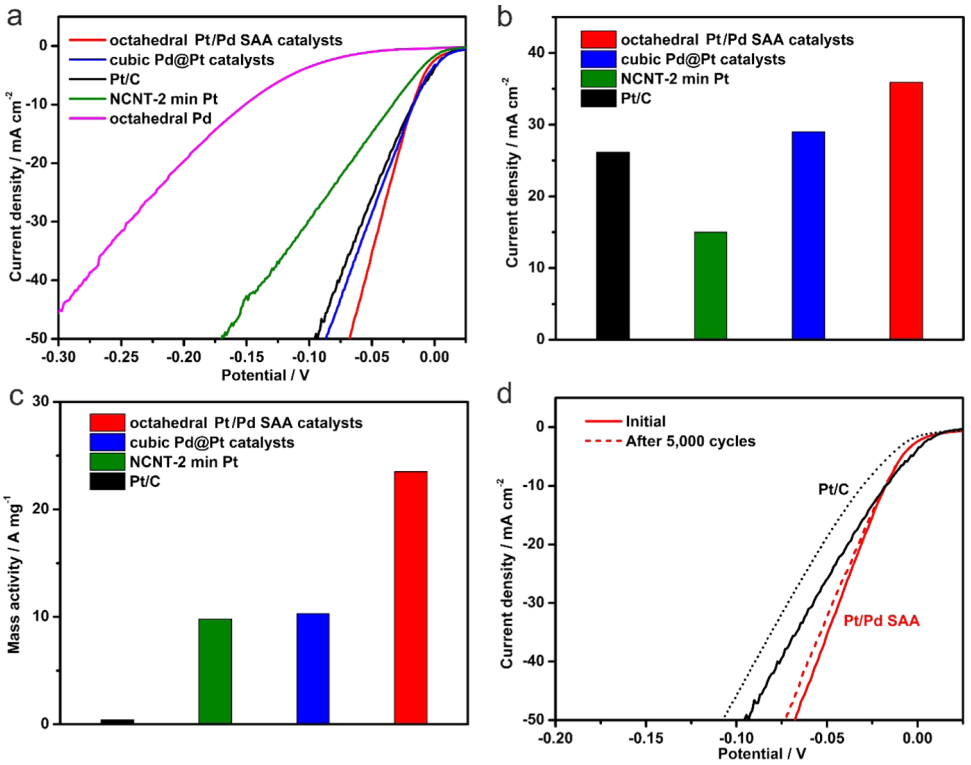

Figure 3. (a) HER polarization curves recorded on the octahedral Pt−Pd SAA, cubic Pd@Pt catalysts, NCNT−2 min Pt, and Pt/C catalysts. (b) Specific activities at 0.05 V of the four types of catalysts, which were normalized to the geometric area of the RDE (0.196 cm^2). (c) Normalized mass activity at 0.05 V. (d) Durability measurement of the octahedral Pt−Pd SAA catalysts and commercial Pt/C catalysts.

atoms other than Pd. In addition, we synthesized Pt atoms on NCNTs with a 2 min pulse time (NCNT−2 min Pt), as shown in Figure S9. NCNT−2 min Pt also exhibited an extremely low current density at 0.9 V vs RHE, indicating that Pt atoms on NCNTs are not active for the ORR (Figure S7b). These results indicated that the activity of octahedral Pt/Pd SAA catalysts can be mostly attributed to the Pt atoms on Pd surfaces. The ORR curves for the as-prepared four types of Pd−Pt catalysts and Pt/C are shown in Figure 2a. To quantitatively compare the activity, we normalized the kinetic current to the Pt mass (Figure 2b) and $ECSA_{Pd+Pt}$ (Figure S10). The kinetic current density (j_k) was calculated by the Koutecky−Levich equation[38] as follows

$$\frac{1}{j} = \frac{1}{j_k} + \frac{1}{j_d}$$

where j is the measured current density and j_d is the diffusion-limiting current density.

When normalized to $ECSA_{Pd+Pt}$, the octahedral Pd−30 min Pt exhibited the best specific activity, which indicates that Pd(111) is much better than Pd(100) as the substrate for improving the activity of Pt atoms. In addition, it can be observed that with the increase of Pt coverage on Pd surfaces, the specific activity of the catalysts can be improved. We also investigated the activities of the catalysts based on Pt mass activity. As shown in Figure 2c, the octahedral Pt/Pd SAA catalysts exhibited the best mass activity, with a mass activity of 0.91 A mg_{Pt}^{-1} at 0.9 V vs RHE, which is around 4 times higher than that of the Pt/C catalyst (0.24 A mg_{Pt}^{-1}). In addition, the octahedral Pt/Pd SAA catalysts exhibited 2.5 times higher activity than the sample with a 30 min pulse time, indicating that the Pt isolated atoms can achieve a greatly improved mass activity compared to the Pt small clusters on Pd particles (Figure 2c). The significant enhancement in mass activity is attributed to the unique SAA structure. It has been proved that the formation of ultrathin Pt shell is an effective route for enhanced Pt mass activity due to their extremely high AUE.[23−26] In our case, the Pt single atoms on octahedral Pd particles exhibited higher activity than the Pt uniform shell on Pd particles. It is worth mentioning that there is a small amount of Pt clusters on Pd surface, which can be considered as partly covered Pd@Pt catalysts. Compared to the octahedral Pd@Pt catalysts (2−3 atomic Pt layers), the as-prepared Pt/Pd SAA still exhibited 2 times higher mass activity. This result further indicates the superior activity of SAA structure. As shown in Table S2, the ORR performance of Pt/Pd SAA catalysts exceeds almost all of the current Pt−Pd bimetallic nanocatalysts with core−shell, nanocage, or alloy structures. For the accelerated durability tests, the ORR polarization curves were measured after sweeping 10 000 cycles between 0.6 and 1.1 V_{RHE} at a scan rate of 0.1 V s^{-1} in an O_2-saturated aqueous $HClO_4$ solution at room temperature. For the mass ORR activities at 0.9 V, the octahedral Pt/Pd SAA catalysts only showed a 14% loss in mass activity (from 0.91 to 0.78 A mg_{Pt}^{-1}) after 5000 cycles (Figure 2d). As a comparison, the commercial Pt/C showed a 41% loss in mass activity (from 0.24 to 0.14 A mg_{Pt}^{-1}) after 5000 cycles. These results indicated that the octahedral Pt/Pd SAA catalysts also exhibit better durability than Pt/C.

The HER activity of the octahedral Pt/Pd SAA catalysts was also measured in comparison to the cubic Pd@Pt catalysts and commercial Pt/C catalysts by conducting linear sweep voltammetry measurements in 0.5 M H_2SO_4 at room temperature. The polarization curves show that the octahedral

DOI: 10.1021/acscatal.9b01677
ACS Catal. 2019, 9, 9350−9358

Pt/Pd SAA catalysts exhibit the best HER performance compared with other types of Pt catalysts, as shown in Figure 3. The specific activity for each catalyst is calculated from the polarization curves by normalizing the current with the geometric area of the electrode (Figure 3a) and $ECSA_{Pd+Pt}$ (Figure S11a). Both the octahedral Pt/Pd SAA catalysts and cubic Pd@Pt catalysts exhibit better specific activity than Pt/C (Figures 3b and S11b). When normalized to the Pt loading, the mass HER activity for the octahedral Pt/Pd SAA catalysts at the overpotential of 0.05 V is 23.5 A mg^{-1}, which is 54.6 times greater than that of the Pt/C catalysts (0.43 A mg^{-1}). It should be pointed out that different from the poor activity for ORR, the NCNT−2 min Pt also exhibited much better performance due to the single-atom structures.[13] In addition, when Pt single atoms are deposited on octahedral Pd, the HER performance can be improved to 23.1 A mg^{-1} at −0.05 V, which further proved the superior activity of SAA structure. We also compared the HER performance of octahedral Pt/Pd SAA catalysts with octahedral Pd−30 min Pt and cubic Pd−30 min Pt catalysts. As shown in Figure S12a, the specific activity of octahedral Pd−30 min Pt and cubic Pd−30 min Pt catalysts is comparable with the 2 min Pt dosing samples. However, when normalized to Pt mass, the octahedral Pt/Pd SAA catalysts and cubic Pd@Pt catalysts exhibited much higher mass activity than the sample with a 30 min pulse time (Figure S12b). Furthermore, the octahedral Pt/Pd SAA catalysts have a superior mass activity compared to other state-of-the-art Pt-based catalysts and current Pt single-atom catalysts (Table S3). These findings suggest that with the deposition of Pt single atoms onto Pd, the SAA structure can significantly increase the HER activity.

To evaluate the durability of the as-prepared SAA catalysts, accelerated degradation tests were adopted between +0.4 and −0.15 V (vs RHE) at 100 mV s^{-1} for 5000 cyclic voltammetry sweeps. As exhibited in Figure 3d, the polarization curve of octahedral Pt/Pd SAA catalysts after 5000 cycles retained a similar performance to the initial test, resulting in a loss of only 9% of its initial current density at an overpotential of 0.05 V. The loss for the Pt/C catalysts was 28% after 5000 cycles at an overpotential of 0.05 V. Due to the strong interaction between Pt atoms with Pd surface, the Pt/Pd SAA catalysts exhibited better stability than the Pt/C catalysts.

3.3. X-ray Adsorption Spectrum Analysis. To further investigate the mechanism of performance enhancement for octahedral Pt/Pd SAA catalysts, we used the X-ray absorption near-edge structure (XANES) and EXAFS spectra to study the electronic structure of this sample. Figures 4a and S13 show that the Pt foil exhibited a substantial intense L_3-edge white line (WL) and a weak L_2-edge WL. While all other samples exhibited substantial WL intensity at both edges. The octahedral Pt/Pd SAA catalysts, cubic Pd@Pt catalysts, and NCNT−2 min Pt appear to have more intense WL compared to Pt foil and octahedral Pd−30 min Pt, which can be related to the highly unoccupied density of Pt 5d states.[12,13] In addition, a small positive shift in the threshold energy E_0 can be observed for the octahedral Pt/Pd SAA catalysts, cubic Pd@Pt catalysts, and NCNT−2 min Pt compared to that for Pt foil. The detailed E_0 position can be determined by the first derivative of the XANES spectrum at the Pt L_3-edge (Figure S14). Among the three as-prepared Pt catalysts, the E_0 for octahedral Pt/Pd SAA catalysts is the one closest to the Pt foil, indicating a metallic property of Pt on octahedral Pd surfaces. As the oxidized Pt will also contribute to the WL intensity, we

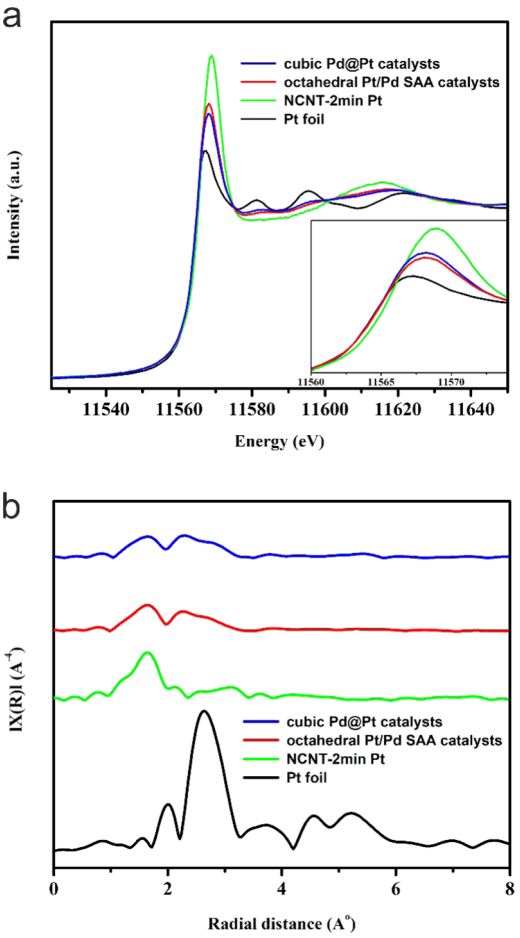

Figure 4. X-ray absorption studies of the octahedral Pt/Pd SAA catalysts, cubic Pd@Pt catalysts, and NCNT−2 min Pt in comparison to Pt foil. (a) Normalized XANES spectra at Pt L_3-edge and (b) K^3-weighted Fourier transform spectra from EXAFS. The inset in A shows the enlarged spectra at Pt L_3-edge.

can speculate that the obtained Pt single atoms are easily oxidized on NCNTs, while the Pt atoms on octahedral Pt are much stable after the ALD process. In addition, we used a reported method to determine the occupancy of the 5d states of Pt quantitatively for each sample.[12,13] As shown in Table 2, the Pt isolated atoms on octahedral Pd particles had an unoccupied density of Pt 5d state character of 0.8176, which is much higher than that of Pt foil sample (0.6754). This result indicates that the interaction between Pt single atoms and Pd surfaces is higher than that of other catalysts.[11−13,39] Due to the strong interaction between Pt and Pd, the Pt/Pd SAA catalysts exhibited enhanced durability compared with Pt/C catalysts.

Furthermore, we analyzed the EXAFS spectra to further study the local atomic structure of Pt. Figure 4b shows the Fourier transforms of the EXAFS region for different samples. A significant peak can be observed at 2.6 Å for Pt foil sample, which is associated with the Pt−Pt peak. The peak at 1.6 Å can be ascribed to Pt bonded to low Z elements (C, O, N). In addition to the two peaks, for the octahedral Pt/Pd SAA catalysts and cubic Pd@Pt samples, a peak located at 2.2 Å can be observed, which can be associated with the Pt−Pd peak. To get detailed coordination information for various samples, we fitted the peaks to quantitatively obtain the coordination number (CN) and bonding length (Figure S15). Table 3

DOI: 10.1021/acscatal.9b01677
ACS Catal. 2019, 9, 9350−9358

Table 2. Pt $L_{3,2}$-Edge Threshold and White Line Parameters

	Pt L_3-edge WL			Pt L_2-edge WL					
sample	E_0 (eV)	E_{Peak} (eV)	ΔA_3	E_0 (eV)	E_{Peak} (eV)	ΔA_3	$h_{5/2}$	$h_{3/2}$	total
Pt foil	11 564	11 567.18	4.75	13 273	13 276	5.68	0.411	0.26	0.6754
NCNT−2 min Pt	11 565.5	11 568.86	5.64	13 273.7	13 276.6	5.56	0.5	0.26	0.756
octahedral Pt/Pd SAA	11 564.5	11 568.06	6.67	13 273.8	13 276.6	4.6	0.6	0.21	0.8176
cubic Pd@Pt catalysts	11 565	11 568.15	6.33	13 273.8	13 276.25	4.3	0.57	0.2	0.773

Table 3. XAS Analysis Results for the Three ALD Samples and Reference Samples

sample	path	coordination number	bond length/Å	$\sigma^2/10^{-3}$ Å^2
Pt foil	Pt−Pt	12	2.76	4.7 (0.2)
NCNT−2 min Pt	Pt−O/C/N	4.12	2.0	5.7 (3.4)
	Pt−Pt			
octahedral Pt/Pd SAA	Pt−O	2.53	2.04	6.5 (2.5)
	Pt−Pd	0.8	2.65	4.1 (3.4)
	Pt−Pt	1.7	2.67	7.7 (7.1)
cubic Pd@Pt catalysts	Pt−O	2	2.01	6.3 (4)
	Pt−Pd	2.7	2.51	7 (5.5)
	Pt−Pt	3.3	2.53	1.9 (0.9)

shows that the Pt−Pt coordination numbers for the octahedral Pt/Pd SAA catalysts and cubic Pd@Pt samples are 1.7 and 3.3, respectively. Due to the formation of Pt isolated atoms and clusters instead of a Pt thin shell on octahedral Pd, the Pt−Pt CN is lower than that on cubic Pd. In addition, we found a fitted Pt−Pd coordination number of 0.8 for the octahedral Pd−2 min Pt, which is much lower than that of cubic Pd−2 min (2.7). This result indicates that Pt atoms on shape-controlled Pd did not diffuse into the crystal lattice of Pd and are located at surface positions. In addition, due to the formation of thin Pt shell on cubic Pd, the Pt−Pt CN occupies a higher surface position than that on octahedral Pd. These results provide more evidence of the presence of isolated Pt atoms on octahedral Pd particles. By adopting the preferred deposition of metallic Pt atoms on octahedral Pd, high density of unoccupied 5d states, and low CN, the Pt atoms exhibited greatly improved ORR activities than Pt/C catalysts.

3.4. Origin of the Enhanced Electrocatalytic Mechanism by DFT. We used density functional theory (DFT) calculations to further investigate the enhanced mechanism of the Pt atoms on Pd surfaces with different structures during the HER and ORR processes. We calculated the Tafel slope of the octahedral Pt/Pd SAA catalysts to be 28.5 dec^{-1} (Figure S16), which can attribute the rate-determining step to the slow atomic combination to form H_2. The whole reaction can be divided into two half-reactions: Volmer steps ($H^+ + e^- \rightarrow H^*$) and Tafel step ($2H^* \rightarrow H_2$). During the Volmer steps, we found that Pt single atom on Pd(111) can strongly absorb H^+ ions. In addition, the high density of unoccupied 5d orbitals (Table 2) can promote the second and third H adsorptions on Pt (Figure 5). As shown in Table S4, the H adsorption energy decreased with the increase of H coverage. The high H coverage on one Pt atom will promote the Tafel process. Therefore, the improved HER activity of Pt/Pd SAA catalysts is due to the highly unoccupied density of states of 5d character and the decreased adsorption energy of H_2 product.

DFT calculation was also used to understand improved ORR performance on the octahedral Pt/Pd SAA catalysts. During the ORR process on Pt, the desorption of OH* is the rate-determining step. Previous studies have shown that the ORR specific activity can be improved by weakening the binding energy of adsorbed OH*.[40,41] We created nanoscale Pt−SAA loaded at Pd octahedra (Pt SAA/Pd(111)) and Pt overlayer on cubic Pd (Pt−OL/Pd(100)) to represent the

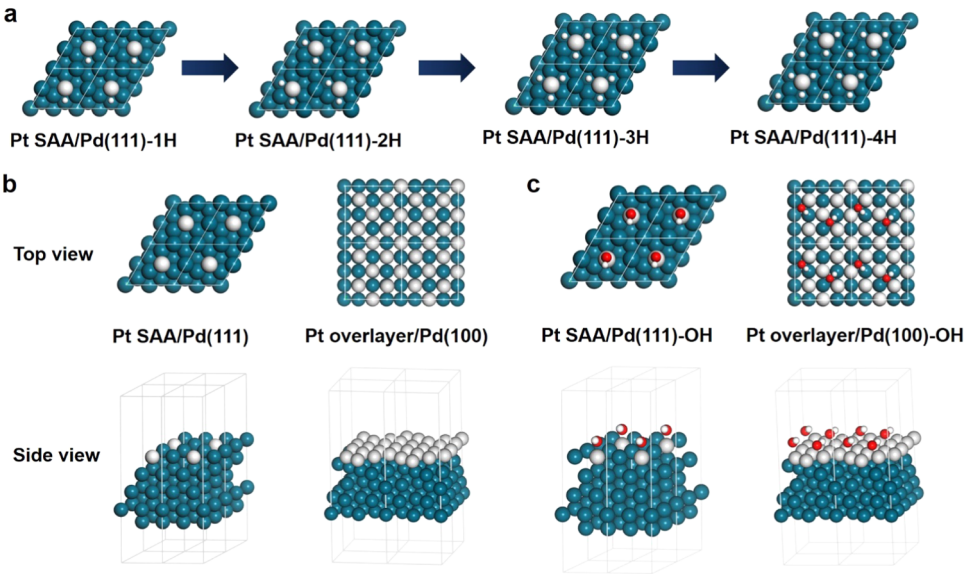

Figure 5. (a) Most stable adsorption configurations of H atoms on Pt−SAA/Pd(111). The coverages of H are 0.25, 0.50, 0.75, and 1.00 ML, respectively. (b) Surface models for Pt−SAA/Pd(111) and Pt−OL/Pd(100). (c) Most stable adsorption configurations of OH on Pt−SAA/Pd(111) and Pt−OL/Pd(100). The coverages of OH are both 0.25 ML.

DOI: 10.1021/acscatal.9b01677
ACS Catal. 2019, 9, 9350−9358

octahedral Pt/Pd SAA and cubic Pd@Pt catalysts, respectively (Figure 5b). The binding energy of OH (BE_{OH}) was calculated on these two models (Figure 5c). The BE_{OH} on Pt−SAA/Pd(111) was calculated to be −2.213 eV, which is much smaller than that of cubic Pd@Pt catalysts (Table S5). This result indicates that the Pt/Pd SAA structure could weaken the interaction between OH* and surface Pt atoms and accelerate ORR kinetics. It was reported that single atomic Ag in AgCu alloys shows very sharp resonances in the valence band spectra, which indicates a free atom-like d state.[42] We also calculate the projected densities of d states of Pt single atoms in Pt/Pd SAA. As shown in Figure S17, Pt single atom in Pt/Pd SAA catalysts does not display the fairly narrowed d states as expected. Instead, the width of d states of Pt in Pt/Pd SAA indeed reduces by about 1 eV compared to that in Pt(111), which is due to the similar electronic properties of Pt and Pd intrinsically. In the future, we will try to synthesize other types of SAA catalysts and do further study between the electronic structures of single atoms and their chemical properties.

4. CONCLUSIONS

In conclusion, we successfully prepared octahedral Pt/Pd SAA catalysts through an ALD process. The as-prepared octahedral Pt/Pd SAA catalysts showed much higher activity compared to the Pt/C catalysts for HER and ORR. The XANES spectrum showed that the obtained Pt atoms on octahedral Pd maintained their metallic state after the ALD process, whereas the Pt atoms could be easily oxidized on NCNTs. The fitted EXAFS spectra provide direct evidence on the presence of isolated Pt atoms on octahedral Pd particles. The formation of SAA structure provided extremely high Pt utilization efficiency, which can effectively improve the mass activity. In addition, the XAS and DFT calculation results indicate that the superior HER activity and stability are also attributed to the relatively high total unoccupied density of states of 5d character and the stable metallic Pt on octahedral Pd particles. The relatively low binding energy of OH on Pt/Pd SAA structure further improved ORR preformation. This study opens up a new avenue of developing new types of Pt-based catalysts for electrocatalytic reactions and brings new understanding about catalytic performances of SAA catalysts.

ASSOCIATED CONTENT

Supporting Information

The Supporting Information is available free of charge on the ACS Publications website at DOI: 10.1021/acscatal.9b01677.

Additional SEM and TEM images; characterization data; cyclic voltammograms; ORR polarization curves; electrochemical impedance spectroscopy; HER polarization curves; normalized XANES spectra; ICP-AES results shows the Pt weight percent in the samples; and comparison of ORR performance (PDF)

AUTHOR INFORMATION

Corresponding Authors

*E-mail: zjzhao@tju.edu.cn (Z.-J.Z.).
*E-mail: gbotton@mcmaster.ca (G.A.B.).
*E-mail: xsun@eng.uwo.ca (X.S.).

ORCID

Hanshuo Liu: 0000-0001-7745-5407
Mohammad Norouzi Banis: 0000-0002-6144-6837
Zhi-Jian Zhao: 0000-0002-8856-5078
Gianluigi A. Botton: 0000-0002-8746-1146
Xueliang Sun: 0000-0003-2881-8237

Author Contributions

⊥L.Z., H.L., and S.L. contributed equally to this work.

Notes

The authors declare no competing financial interest.

ACKNOWLEDGMENTS

This work was supported by the Natural Sciences and Engineering Research Council of Canada (NSERC), Canada Research Chair (CRC) Program, Canada Foundation for Innovation (CFI), and the University of Western Ontario. The electron microscopy characterization was carried out at the Canadian Centre for Electron Microscopy (CCEM), a national facility supported by NSERC, the Canada Foundation for Innovation (via the MSI program), and McMaster University.

REFERENCES

(1) Tian, N.; Zhou, Z. Y.; Sun, S. G.; Ding, Y.; Wang, Z. L. Synthesis of Tetrahexahedral Platinum Nanocrystals with High-Index Facets and High Electro-Oxidation Activity. *Science* **2007**, *316*, 732−735.

(2) Gan, L.; Cui, C.; Heggen, M.; Dionigi, F.; Rudi, S.; Strasser, P. Element-Specific Anisotropic Growth of Shaped Platinum Alloy Nanocrystals. *Science* **2014**, *346*, 1502−1506.

(3) Zhang, L.; Roling, L. T.; Wang, X.; Vara, M.; Chi, M.; Liu, J.; Choi, S.-I.; Park, J.; Herron, J. A.; Xie, Z.; Mavrikakis, M.; Xia, Y. Platinum-Based Nanocages with Subnanometer-Thick Walls and Well-Defined, Controllable Facets. *Science* **2015**, *349*, 412−416.

(4) Chen, C.; Kang, Y.; Huo, Z.; Zhu, Z.; Huang, W.; Xin, H. L.; Snyder, J. D.; Li, D.; Herron, J. A.; Mavrikakis, M.; Chi, M.; More, K. L.; Li, Y.; Markovic, N. M.; Somorjai, G. A.; Yang, P.; Stamenkovic, V. R. Highly Crystalline Multimetallic Nanoframes with Three-Dimensional Electrocatalytic Surfaces. *Science* **2014**, *343*, 1339−1343.

(5) Li, M.; Zhao, Z.; Cheng, T.; Fortunelli, A.; Chen, C.-Y.; Yu, R.; Zhang, Q.; Gu, L.; Merinov, B. V.; Lin, Z.; Zhu, E.; Yu, T.; Jia, Q.; Guo, J.; Zhang, L.; Goddard, W. A., III; Huang, Y.; Duan, X. Ultrafine Jagged Platinum Nanowires Enable Ultrahigh Mass Activity for the Oxygen Reduction Reaction. *Science* **2016**, *354*, 1414−1419.

(6) Shao, M.; Peles, A.; Shoemaker, K. Electrocatalysis on Platinum Nanoparticles: Particle Size Effect on Oxygen Reduction Reaction Activity. *Nano Lett.* **2011**, *11*, 3714−3719.

(7) Nesselberger, M.; Ashton, S.; Meier, J. C.; Katsounaros, I.; Mayrhofer, K. J. J.; Arenz, M. The Particle Size Effect on the Oxygen Reduction Reaction Activity of Pt Catalysts: Influence of Electrolyte and Relation to Single Crystal Models. *J. Am. Chem. Soc.* **2011**, *133*, 17428−17433.

(8) Yang, S.; Kim, J.; Tak, Y. J.; Soon, A.; Lee, H. Single-Atom Catalyst of Platinum Supported on Titanium Nitride for Selective Electrochemical Reactions. *Angew. Chem., Int. Ed.* **2016**, *55*, 2058−2062.

(9) Li, X.; Bi, W.; Zhang, L.; Tao, S.; Chu, W.; Zhang, Q.; Luo, Y.; Wu, C.; Xie, Y. Single-Atom Pt as Co-Catalyst for Enhanced Photocatalytic H_2 Evolution. *Adv. Mater.* **2016**, *28*, 2427−2431.

(10) Liu, J.; Jiao, M.; Lu, L.; Barkholtz, H. M.; Li, Y.; Wang, Y.; Jiang, L.; Wu, Z.; Liu, D.-J.; Zhuang, L.; Ma, C.; Zeng, J.; Zhang, B.; Su, D.; Song, P.; Xing, W.; Xu, W.; Wang, Y.; Jiang, Z.; Sun, G. High Performance Platinum Single Atom Electrocatalyst for Oxygen Reduction Reaction. *Nat. Commun.* **2017**, *8*, No. 15938.

(11) Qiao, B.; Wang, A.; Yang, X.; Allard, L. F.; Jiang, Z.; Cui, Y.; Liu, J.; Li, J.; Zhang, T. Single-Atom Catalysis of CO Oxidation Using Pt_1/FeO_x. *Nat. Chem.* **2011**, *3*, 634−641.

(12) Sun, S.; Zhang, G.; Gauquelin, N.; Chen, N.; Zhou, J.; Yang, S.; Chen, W.; Meng, X.; Geng, D.; Banis, M.; Li, R.; Ye, S.; Knights, S.; Botton, G.; Sham, T.-K.; Sun, X. Single-Atom Catalysis Using Pt/

DOI: 10.1021/acscatal.9b01677
ACS Catal. 2019, 9, 9350−9358

Graphene Achieved Through Atomic Layer Deposition. *Sci. Rep.* **2013**, *3*, No. 1775.
(13) Cheng, N.; Stambula, S.; Wang, D.; Banis, M.; Liu, J.; Riese, A.; Xiao, B.; Li, R.; Sham, T.-K.; Liu, L.; Botton, G.; Sun, X. Platinum Single-Atom and Cluster Catalysis of the Hydrogen Evolution Reaction. *Nat. Commun.* **2016**, *7*, No. 13638.
(14) Yan, H.; Lin, Y.; Wu, H.; Zhang, W.; Sun, Z.; Cheng, H.; Liu, W.; Wang, C.; Li, J.; Huang, X.; Yao, T.; Yang, J.; Wei, S.; Lu, J. Bottom-Up Precise Synthesis of Stable Platinum Dimers on Graphene. *Nat. Commun.* **2017**, *8*, No. 1070.
(15) Li, H.; Wang, L.; Dai, Y.; Pu, Z.; Lao, Z.; Chen, Y.; Wang, M.; Zheng, X.; Zhu, J.; Zhang, W.; Si, R.; Ma, C.; Zeng, J. Synergetic Interaction between Neighbouring Platinum Monomers in CO_2 Hydrogenation. *Nat. Nanotechnol.* **2018**, *13*, 411−417.
(16) Yan, C.; Li, H.; Ye, Y.; Wu, H.; Cai, F.; Si, R.; Xiao, J.; Miao, S.; Xie, S.; Yang, F.; Li, Y.; Wang, G.; Bao, X. Coordinatively Unsaturated Nickel−Nitrogen Sites towards Selective and High-Rate CO_2 Electroreduction. *Energy Environ. Sci.* **2018**, *11*, 1204−1210.
(17) Pan, Y.; Lin, R.; Chen, Y.; Liu, S.; Zhu, W.; Cao, X.; Chen, W.; Wu, K.; Cheong, W. C.; Wang, Y.; Zheng, L.; Luo, J.; Lin, Y.; Liu, Y.; Liu, C.; Li, J.; Lu, Q.; Chen, X.; Wang, D.; Peng, Q.; Chen, C.; Li, Y. Design of Single-Atom Co-N_5 Catalytic Site: A Robust Electrocatalyst for CO_2 Reduction with nearly 100% CO Selectivity and Remarkable Stability. *J. Am. Chem. Soc.* **2018**, *140*, 4218−4221.
(18) Liu, J.; Lucci, F. R.; Yang, M.; Lee, S.; Marcinkowski, M. D.; Therrien, A. J.; Williams, C. T.; Sykes, E. C. H.; Flytzani-Stephanopoulos, M. Tackling CO Poisoning with Single-Atom Alloy Catalysts. *J. Am. Chem. Soc.* **2016**, *138*, 6396−6399.
(19) Lucci, F. R.; Liu, J.; Marcinkowski, M. D.; Yang, M.; Allard, L. F.; Flytzani-Stephanopoulos, M.; Sykes, E. C. H. Selective Hydrogenation of 1,3-Butadiene on Platinum-Copper Alloys at the Single-Atom Limit. *Nat. Commun.* **2016**, *6*, No. 8850.
(20) Marcinkowski, M. D.; Liu, J.; Murphy, C. J.; Liriano, M. L.; Wasio, N. A.; Lucci, F. R.; Flytzani-Stephanopoulos, M.; Sykes, E. C. H. Selective Formic Acid Dehydrogenation on Pt-Cu Single-Atom Alloys. *ACS Catal.* **2017**, *7*, 413−420.
(21) Marcinkowski, M. D.; Darby, M. T.; Liu, J.; Wimble, J. M.; Lucci, F. R.; Lee, S.; Michaelides; Flytzani-Stephanopoulos, A. M.; Stamatakis, M.; Sykes, E. C. H. Pt/Cu Single-Atom Alloys as Coke-Resistant Catalysts for Efficient C-H Activation. *Nat. Chem.* **2018**, *10*, 325−332.
(22) Sun, G.; Zhao, Z.-J.; Mu, R.; Zha, S.; Li, L.; Chen, S.; Zang, K.; Luo, J.; Li, Z.; Purdy, S. C.; Kropf, A. J.; Miller, J. T.; Zeng, L.; Gong, J. Breaking the Scaling Relationship via Thermally Stable Pt/Cu Single Atom Alloys for Catalytic Dehydrogenation. *Nat. Commun.* **2018**, *9*, No. 4454.
(23) Park, J.; Zhang, L.; Choi, S.-I.; Roling, L. T.; Lu, N.; Herron, J. A.; Xie, S.; Wang, J.; Kim, M. J.; Mavrikakis, M.; Xia, Y. Atomic Layer-by-Layer Deposition of Platinum on Palladium Octahedra for Enhanced Catalysts toward the Oxygen Reduction Reaction. *ACS Nano* **2015**, *9*, 2635−2647.
(24) Xie, S.; Choi, S.-I.; Lu, N.; Roling, L. T.; Herron, J. A.; Zhang, L.; Park, J.; Wang, J.; Kim, M. J.; Xie, Z.; Mavrikakis, M.; Xia, Y. Atomic Layer-by-Layer Deposition of Pt on Pd Nanocubes for Catalysts with Enhanced Activity and Durability toward Oxygen Reduction. *Nano Lett.* **2014**, *14*, 3570−3576.
(25) Bian, T.; Zhang, H.; Jiang, Y.; Jin, C.; Wu, J.; Yang, H.; Yang, D. Epitaxial Growth of Twinned Au-Pt Core-Shell Star-Shaped Decahedra as Highly Durable Electrocatalysts. *Nano Lett.* **2015**, *15*, 7808−7815.
(26) Wang, X.; Choi, S.-I.; Roling, L. T.; Luo, M.; Ma, C.; Zhang, L.; Chi, M.; Liu, J.; Xie, Z.; Herron, J. A.; Mavrikakis, M.; Xia, Y. Palladium-Platinum Core-Shell Icosahedra with Substantially Enhanced Activity and Durability towards Oxygen Reduction. *Nat. Commun.* **2015**, *6*, No. 7594.
(27) Wu, J.; Qi, L.; You, H.; Gross, A.; Li, J.; Yang, H. Icosahedral Platinum Alloy Nanocrystals with Enhanced Electrocatalytic Activities. *J. Am. Chem. Soc.* **2012**, *134*, 11880−11883.
(28) Wang, X.; Vara, M.; Luo, M.; Huang, H.; Ruditskiy, A.; Park, J.; Bao, S.; Liu, J.; Howe, J.; Chi, M.; Xie, Z.; Xia, Y. Pd@Pt Core-Shell Concave Decahedra: A Class of Catalysts for the Oxygen Reduction Reaction with Enhanced Activity and Durability. *J. Am. Chem. Soc.* **2015**, *137*, 15036−15042.
(29) He, D. S.; He, D.; Wang, J.; Lin, Y.; Yin, P.; Hong, X.; Wu, Y.; Li, Y. Ultrathin Icosahedral Pt-Enriched Nanocage with Excellent Oxygen Reduction Reaction Activity. *J. Am. Chem. Soc.* **2016**, *138*, 1494−1497.
(30) Jin, M.; Zhang, H.; Xie, Z.; Xia, Y. Palladium Nanocrystals Enclosed by {100} and {111} Facets in Controlled Proportions and Their Catalytic Activities for Formic Acid Oxidation. *Energy Environ. Sci.* **2012**, *5*, 6352−6357.
(31) Bulusheva, L. G.; Okotrub, A. V.; Kurenya, A. G.; Zhang, H.; Zhang, H.; Chen, X.; Song, H. Electrochemical Properties of Nitrogen-Doped Carbon Nanotube Anode in Li-Ion Batteries. *Carbon* **2011**, *49*, 4013−4023.
(32) Kresse, G.; Furthmüller, J. Efficient Iterative Schemes for *ab initio* Total-Energy Calculations using a Plane-Wave Basis Set. *Phys. Rev. B* **1996**, *54*, No. 11169.
(33) Wellendorff, J.; Lundgaard, K. T.; Møgelhøj, A.; Petzold, V.; Landis, D. D.; Nørskov, J. K.; Bligaard, T.; Jacobsen, K. W. Density Functionals for Surface Science: Exchange-Correlation Model Development with Bayesian Error Estimation. *Phys. Rev. B* **2012**, *85*, No. 235149.
(34) Haynes, W. M. *CRC Handbook of Chemistry and Physics*, 94th ed.; Taylor and Francis: Boca Raton, 2014.
(35) Greeley, J.; Mavrikakis, M. Alloy Catalysts Designed from First Principles. *Nat. Mater.* **2004**, *3*, 810−815.
(36) Mavrikakis, M.; Hammer, B.; Nørskov, J. K. Effect of Strain on the Reactivity of Metal Surfaces. *Phys. Rev. Lett.* **1998**, *81*, 2819−2822.
(37) Bligaard, T.; Nørskov, J. K. Ligand Effects in Heterogeneous Catalysis and Electrochemistry. *Electrochim. Acta* **2007**, *52*, 5512−5516.
(38) Gasteiger, H. A.; Kocha, S. S.; Sompalli, B.; Wagner, F. T. Fuel Processing and PEM Fuel Cells: Advanced Catalysts, Adsorbents and Electrocatalysts. *Appl. Catal., B* **2005**, *56*, 9−35.
(39) Hu, P.; Huang, Z.; Amghouz, Z.; Makkee, M.; Xu, F.; Kapteijn, F.; Dikhtiarenko, A.; Chen, Y.; Gu, X.; Tang, X. Electronic Metal-Support Interactions in Single-Atom Catalysts. *Angew. Chem., Int. Ed.* **2014**, *53*, 3418−3421.
(40) Zhao, Z.-J.; Mu, R.; Wang, X.; Gong, J. Fast Prediction of CO Binding Energy via the Local Structure Effect on PtCu Alloy Surfaces. *Langmuir* **2017**, *33*, 8700−8706.
(41) Greeley, J.; Stephens, I. E. L.; Bondarenko, A. S.; Johansson, T. P.; Hansen, H. A.; Jaramillo, T. F.; Rossmeisl, J.; Chorkendorff, I.; Nørskov, J. K. Alloys of Platinum and Early Transition Metals as Oxygen Reduction Electrocatalysts. *Nat. Chem.* **2009**, *1*, 552−556.
(42) Greiner, M. T.; Jones, T. E.; Beeg, S.; Zwiener, L.; Scherzer, M.; Girgsdies, F.; Piccinin, S.; Armbrüster, M.; Knop-Gericke, A.; Schlögl, R. Free-atom-like d states in single-atom alloy catalysts. *Nat. Chem.* **2018**, *10*, 1008−1015.

DOI: 10.1021/acscatal.9b01677
ACS Catal. 2019, 9, 9350−9358